Beyond efficiency: Phenothiazine, a new commercially viable substituent for hole transport materials for perovskite solar cells

Journal Name

ARTICLE

Beyond efficiency: Phenothiazine, a new commercially viable substituent for hole transport materials for perovskite solar cells

Michal R. Maciejczyk,[a] Ruihao Chen,[b] Alasdair Brown,[a] Nanfeng Zheng*[a] and Neil Robertson*[a]

Received 00th January 20xx,
Accepted 00th January 20xx

DOI: 10.1039/x0xx00000x

www.rsc.org/

Two triphenylbenzene (TPB) derivatives, 1,3,5-Tris(2'-((N,N-di(4-methoxyphenyl)amino)phenyl)benzene (TPB(2-MeOTAD)) and 1,3,5-Tris(2'-(N-phenothiazylo)phenyl)benzene (TPB(2-TPTZ)) have been synthesized via two cost-efficient two step process, and fully characterized by $^{1}H/^{13}C$ NMR spectroscopy and mass spectrometry. For the first time in perovskite solar cells, phenothiazine has been introduced, as a low cost substituent to replace commonly used dimethoxydiphenylamine- which consitute of almost 90% of the final cost of hole transporting materials (HTMs). The use of a more flexible central core than state of the art spirobifluorene (SBF) lowers the highest occupied molecular orbital (HOMO) energy level, increases solubility and decreases the glass transition temperature. The derivatives were employed as hole-transport materials, and their performances were compared via the fabrication of mesoporous ZnO-Mg-EA(NH_3^+)/$CH_3NH_3PbI_3$/HTM/Au solar cells. The best cells obtained have a optimized PCE of 12.14% and 4.32% for cells based on 4,4'-dimethoxydiphenylamine and phenothiazine substituent, respectively. Due to the extremely low cost of TPB(2-TPTZ) equal to 3.43 \$/g, in solar cells it delivers the lowest cost per peak Watt of 0.014 $/$W_p$, which is 15 times lower than spiro-MeOTAD. This shows that the approach is commercially viable with potential to deliver HTM with cost contribution to final module as little as 1%.

Introduction

Organic-inorganic lead halide perovskite solar cells (PSCs), due to superior attributes like high efficiency, low cost and simple manufacturing with possible roll-to-roll processing, have attracted significant attention both in academia and in industry.[1–3] The typical structure of PSCs includes the light-absorbing layer sandwiched between electron transport material (ETM) and hole transport material (HTM). The role of the HTM is to facilitate hole extraction and retard charge recombination at the interface between the HTM and the perovskite layer. To fulfil these requirements ideal materials have good hole transport capacity and conductivity, high mobility,[4] the highest occupied molecular orbital (HOMO) energy level should be well aligned with the valence band of the perovskite material,[5] good solubility to facilitate processability and low cost to justify its use.[6]

The most commonly used state-of-the-art HTM 2,2',7,7'-tetrakis-(N,N-di-pmethoxyphenylamine)-9,9'–spirobifluorene (*spiro*-OMeTAD) can deliver efficiency as high as 22.0%[7], which is close to the record certified efficiency 22.7%,[8] but its tedious multistep synthesis and complicated doping process to achieve sufficient conductivity, leading to high price and low stability stimulates further research to find more cost efficient and dopant-free candidates. To fulfil these requirements numerous novel hole transport materials have been introduced. For instance, the most recent reports with the reference device efficiency based on *spiro*-OMeTAD given in parentheses, includes structures like: spiro[fluorene-9,9'-phenanthren-10-one]-16.06% (16.08%);[9] spiro[dibenzo[*c*,*h*]xanthene-7,9'-fluorene]- 15.9% (10.8%) for undoped HTMs;[10] 2,5,9,12-tetra(*tert*-butyl)diacenaphtho[1,2-*b*:1',2'-*d*]thiophenen with 15.59% (16.5%-doped) and 18.17% (18.30%-doped) efficiencies for undoped HTM with n-i-p planar and mesoscopic architectures, respectively;[11] carbazole modified fluorene branched structures- 18.3% (18.9%);[12] diphenylamine substituted carbazole- 18.92% (18.79%);[13] anthanthrone based HTMs with 17.5% (16.8%-doped) efficiency for undoped HTMs;[14] pyrene based HTMs- 18.23% (16.00%);[15] phenothiazine based HTMs- 19.17% (19.66%);[16] fluoranthene based HTMs with 18.03% (9.33%) efficiency for undoped HTMs;[17] fluorene terminated spiro HTMs with 22.3% (21.3%) efficiency.[18] Thereby, showing that, by proper molecular engineering, comparable or even greater efficiency than for *spiro*-MeOTAD can be achieved, especially when no dopants are used.

Our recent findings[6] on PSCs with architecture TiO_2/ mesoAl_2O_3/ $MAPbI_{3-x}Cl_x$/ HTM showed that interchange of the core unit from SpiroMeOTAD, namely spirobifluorene (SBF) with the product of one-pot reaction of fluorenone and phenol in the presence of methanesulfonic acid without any solvent spiro[fuorene-9,9'-xanthene] (SFX) to give SFX-MeOTAD[19] leads to comparable power conversion efficiency (PCE) but more than 5 times lower cost. This material, also simultaneously reported

[a] School of Chemistry and EaStCHEM, University of Edinburgh, King's Buildings, David Brewster Road, Edinburgh, Scotland EH93FJ, UK. E-mail: Neil.Robertson@ed.ac.uk
[b] State Key Laboratory of Physical Chemistry of Solid Surfaces, Xiamen University, 422 Siming South Road, Xiamen, Fujian 361005, P. R. China, Email: nfzheng@xmu.edu.cn

† Electronic Supplementary Information (ESI) available: DSC and TGA curves, electrochemical characteristics, XRD powder patterns, device performance, solubility studies, H^1 and C^{13} NMR spectra. See DOI: 10.1039/x0xx00000x

as X60,[20] has been independently investigated by other researchers as a HTM for PSCs to give efficiency of 19.8% (TiO_2/ nc-TiO_2/ $FAPbI_3$-PbI_2-MABr-$PbBr_2$/ HTM),[20] 16.8% (TiO_2/ mesoTiO$_2$/ $MAPbI_3$/ HTM) and 17.7% (TiO_2/mesoTiO$_2$/ $FAPbI_3$-$MAPbBr_3$/ HTM),[21] 19.0% (TiO_2/ mesoTiO$_2$/ $FAPbI_3$-$MAPbBr_3$/ HTM(TFSI)$_2$)[22] or to study charge transfer dynamics and effects of molecular symmetry.[23,24] Leaving SFX-MeOTAD the second most studied low molecular HTM, as successor to Spiro-MeOTAD. However, the need to match the HOMO energy level of the HTM with the valence band maxima of a variety of perovskites with larger bandgaps calls for further development of HTMs with tuned HOMO energies. Unfortunately, utilizing substituents other than 4,4'-dimethoxydiphenylamine on the SFX core, like carbazole or phenothiazine with significantly lower HOMO levels, leads to insoluble materials. To solve this problem Chiykowski et al. have studied the influence of selective placement of 4,4'-dimethoxydiphenylamine onto the SFX core leading to control over hole mobility, glass transition temperature and HOMO level, achieving power conversion efficiency (PCE) of 20.8%.[25] The cost of the substituent materials however, is also an important factor. The commercial price was estimated (based on cheapest offer and the largest quantity available from common suppliers) to be 6.80 $/g for 4,4'-dimethoxydiphenylamine, 0.02 $/g for phenothiazine and 0.19 $/g for carbazole. It is clear that phenothiazine in particular is very cost-effective material, as it can be purchased in kilogram quantities, over 300 times less expensive than 4,4'-dimethoxydiphenylamine which according to our previous cost estimation[6] accounts for almost 90 % of the material's cost of Buchwald-Hartwig amination. Additionally, sulfur based heterocycles have been found to strengthen the interaction between the perovskite and HTM,[16,26–28] however the low solubility of phenothiazine and carbazole-substituted molecules has limited their use in hole-transport materials for PSCs. Therefore, developing materials that do not require this pricy substituent at all, or can use cost effective analogues that can also tune HOMO levels, is of high interest. As has been discussed by Osedach et al.,[29] to make materials for organic photovoltaics commercially viable, the synthesis has to be scaled to thousands of kilograms. Moreover, the cost of the material has to be small, normally requiring a small number of synthetic steps, as the cost increase linearly with the number of steps. Thus, high efficiency in solar cells shows the prospects for the technology but does not indicate its commercial viability. The authors of the paper cited above concluded that material costs for organic photovoltaics should be in the range of 1-10% of the module cost. This puts restrictions on the individual active layer price, which should be less than 0.005 or 0.050 $/W$_p$. The importance of the cost of the hole transporting material for perovskite solar cells has been well identified by researchers and targeted in a number of publications, but the main emphasis has been mainly on designing new cores that utilize 4,4'-dimethoxydiphenylamine as a substituent which delivers the desirable HOMO energy level.

Therefore, in our work we have introduced, for the first time in perovskite solar cells, phenothiazine as a low cost substituent to replace the almost-exclusively used 4,4'-dimethoxydiphenylamine. We report synthesis, photophysical and device studies of a novel approach to easily accessible *ortho* substituted triphenylbenzene (**TPB**) based hole conductors. The materials presented possess high solubility, good thermal stability and low HOMO level around -5.3 eV. The fabricated devices (non-optimized) have a PCE of 12.14% and 4.32% for cells based on 4,4'-dimethoxydiphenylamine and phenothiazine substituent, respectively and further optimization may significantly improve device performances. We have implemented these materials in a recently developed novel device structure which replaces the typically-used electron transporting material, titanium dioxide, with ZnO ETL modified with a thin layer of MgO and a sub-monolayer of protonated ethanolamine (EA); this architecture has been optimized up to a high efficiency of 21.1 % and no hysteresis when *spiro*-MeOTAD HTM has been utilized.[30]

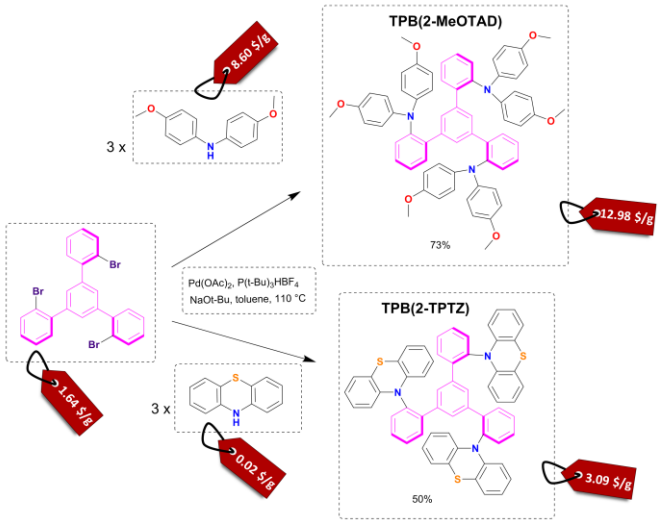

Fig. 1 Reaction scheme for the Buchwald-Hartwig amination of 1, 3, 5-tris(2-bromophenyl) benzene with 4, 4'-dimethoxydiphenylamine and phenothiazine with estimated cost on the price tag.

Results and discussion

Synthetic procedures and characterization

The starting material for this reaction, 1,3,5-tris(2-bromophenyl) benzene, is not commercially available. However, it can be simply synthesised by an aldol condensation reaction of 2'-bromoacetophenone with cost efficient and accessible reagent-silicon tetrachloride.[31] The next and final step (**Fig. 1**) leading to the novel hole transporting materials used Buchwald-Hartwig coupling with good 73% to moderate 50% reaction yield for **TPB(2-MeOTAD)** and **TPB(2-TPTZ)**, respectively. Thus, the complexity of the synthetic procedures required to produce these materials was low throughout. All of the analytical data (^{1}H/^{13}C NMR spectroscopy, mass spectrometry and elemental analysis) can be found in the Electronic Supporting Information (ESI).

To asses material cost of the HTM we have used a procedure reported by Osedach *et al*. for materials for organic

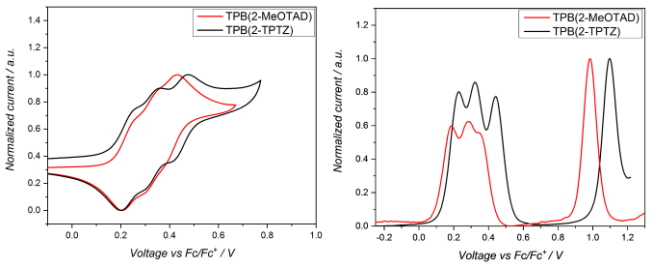

Fig. 2 Cyclic voltammograms (CV) (left) and Square Wave Voltammetry (SWV) of TPB(2-MeOTAD) and TPB(2-TPTZ) in DCM solution with supporting electrolyte 0.3 M tetrabutylammonium hexafluorophosphate referenced to ferrocene.

photovoltaics and followed work by Petrus *et. al*. which introduced it to the field of HTMs for perovskites.[29,32,33] We have simplified the cost estimation by omitting costs of workup and purification since on the small scale chlorinated solvents and column chromatography increase the cost of the final material significantly but these steps would be substituted by appropriate solvent choice and recrystallization procedure on the process development stage. The estimated cost of the materials for the central 1,3,5-Tris(2-bromophenyl)benzene core is 1.64 $/g; for the final HTMs we found 12.98 $/g and 3.09 $/g for TPB(2-MeOTAD) and TPB(2-TPTZ), respectively (see ESI from more details). These costs are much lower than the price of state-of-the-art spiro-MeOTAD which can be within the range of 100 to 400 $/g. Such a low materials costs comes from only two reactions steps and low precursor costs. In particular, the phenothiazine substituent has tremendous potential due to extremely low cost of only 0.02 $/g which constitute only 1% of the cost in comparison with around 85% for dimethoxydiphenylamine. At the same time TPB(2-TPTZ) has a good match of its HOMO energy level with the valence band of the perovskite absorber.

The solubility of all three products was assessed in three different solvents: chlorobenzene, chloroform and toluene. Both materials were easily soluble in chloroform, toluene and chlorobenzene (Table S 2, ESI) with the lowest solubility for **TPB(2-MeOTAD)** of 50mg/ml in chlorobenzene and the highest solubility for **TPB(2-TPTZ)** of 260 mg/ml in chloroform and moderate solubility for both of materials in toluene at the level of 150 mg/ml. This contrasts with our previously reported[6] derivatives based on SFX core with phenothiazine and carbazole substituents which showed very low solubility of less than 10 mg/ml. Even although, the addition of an oxygen atom to change the SBF spiro-structure into the SFX brings improved solubility and processability, this effect is insufficient when more planar substituents are introduced. Thus, it is clear that the triphenylbenzene core improves solubility dramatically, attributed to the free rotation of the bonds between the central benzene and the phenyl groups typical in TPBs. This should enable the molecule to dissolve more easily as it has more freedom to reorient in solution. As such, even when the rigid, planar phenothiazine was employed, the solubility of the hole transport material was retained. All of these factors are advantages for the scalability of the reaction and materials accessibility since solubilizing groups on the amine derivatives

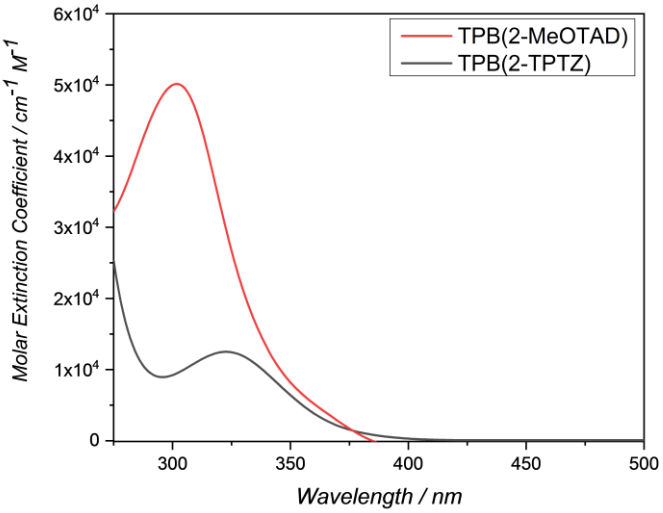

Fig. 3 UV/Visible absorption of TPB(2-MeOTAD) and TPB(2-TPTZ) in diluted DCM.

are not required as they would be the case of the spiro core. This is particularly relevant for the phenothiazine substituent, which has been recently used to prepare HTMs of high thermal stability, large Stokes shift and hole mobility of 2.08×10^{-3} $cm^2V^{-1}S^{-1}$ with the energy level very well matched with $CH_3NH_3PbI_3$ but suffering from impractically low solubility.[34]

Electrochemical and optical properties

Cyclic voltammetry was run between -2.00 and +2.00 V to check for reduction processes at negative potential (Fig. S3, ESI). None were visible for either material in the solvent window used. Therefore, the LUMO energy levels could not be estimated from electrochemical data. The oxidation potentials (E_{OX}) of **TPB(2-MeOTAD)** and **TPB(2-TPTZ)** were elucidated by cyclic and square-wave voltammetry. Against ferrocene/ferrocenium as the internal standard, the oxidation potentials of **TPB(2-MeOTAD)** and **TPB(2-TPTZ)** were 0.19 V and 0.24 V respectively. These values were used to estimate the energy of the highest occupied molecular orbital (E_{HOMO}) of each material. Accordingly, **TPB(2-MeOTAD)** and **TPB(2-TPTZ)** gave E_{HOMO} values of -5.29 eV and -5.34 eV respectively. Both values are clearly lower than the benchmark material ***spiro*-MeOTAD** (-5.14 eV). Thus, **TPB(2-MeOTAD)** and **TPB(2-TPTZ)** have E_{HOMO} levels which are closer in energy to the valence band of $MAPbI_3$ (-5.44 eV), the most commonly employed Perovskite material. This indicates that hole injection from $MAPbI_3$ is favourable. Furthermore, as the open-circuit voltage (V_{OC}) is strongly linked to the difference between the quasi-Fermi level of the electron transport material and the HOMO level of the HTM,[35] the lower E_{HOMO} could increase the V_{OC}. The cyclic and square wave voltammetry plots against ferrocene for each material are shown in Fig. 2 and the peaks are tabulated in Table 1. The electrochemical reversibility of each oxidation process was assessed by running measurements at different scan rates (Fig. S1, ESI). For both **TPB(2-MeOTAD)** and **TPB(2-TPTZ)**, E_{pa} and E_{pc} were found to be independent of scan rate and I_{pa} and I_{pc} showed a linear dependence on the square root of the scan rate

(Fig. S2, ESI). Thus, the oxidation peaks for both materials were electrochemically reversible.

Table 1 Electrochemical, photophysical and thermal properties.

Name	λ_{abs}[a] nm	ε[a] $\times 10^3$, $cm^{-1}M^{-1}$	E_{gap} eV[ab]	HOMO[c]	LUMO[d]	E_{ox}[a] V	T_g[e] °C	T_m[e] °C	T_d[f] °C
TPB(2-MeOTAD)	300	50	3.54	-5.29	-1.75	0.19	89	181	436
TPB(2-TPTZ)	323	12.5	3.32	-5.34	-2.02	0.24	110	251	448

[a] In dichloromethane solution. [b] Optical gap, from intersection of Abs and Pl. [c] E_{HOMO}= -5.1 - (E_{ox}).[36] [d] E_{LUMO}= E_{HOMO} + E_{gap}. [e] Glass transition temperature (T_g) and melting point (T_m) by DSC. [f] Decomposition temperature (T_d) by TGA.

UV-Visible spectroscopy was conducted on **TPB(2-MeOTAD)** and **TPB(2-TPTZ)** in dichloromethane (Fig. 3). Both absorb in the UV region, with maximum absorption wavelengths of 300 and 323 nm, respectively. The optical band gaps (E_{gap}) were estimated from the onset of absorption. From these E_{gap} values and the E_{HOMO} values gathered from electrochemistry, the energy of the lowest unoccupied molecular orbitals (E_{LUMO}) were estimated.

Thermal analysis

Differential Scanning Calorimetry (DSC) was conducted for **TPB(2-MeOTAD)** and **TPB(2-TPTZ)** (Fig. S4 and S6, ESI). Glass transitions were recorded at 89 and 110 °C for **TPB(2-MeOTAD)** and **TPB(2-TPTZ)** respectively. The dimethoxydiphenylamine substituent is comprised of two independently-flexible phenyl rings, whereas the entire phenothiazine substituent must arrange as a single unit. It is probable that this greater rigidity and planarity on **TPB(2-TPTZ)** inhibits organisation into a crystal structure, hence greater thermal energy was required to destabilise the amorphous state. The glass transitions of both materials are lower than ***spiro*-MeOTAD** (122 °C). Melting points were observed for both; **TPB(2-MeOTAD)** melted at 181 °C, **TPB(2-TPTZ)** at 251 °C. This value for **TPB(2-TPTZ)** is higher than that of ***spiro*-MeOTAD**, confirming that it has high thermal stability

Thermal Gravimetric Analysis (TGA) of **TPB(2-MeOTAD)** and **TPB(2-TPTZ)** indicated that both were thermally stable with respect to decomposition (Fig. S5 and S7, ESI). Mass loss of 5% occurred at 436 °C for **TPB(2-MeOTAD)** and 448 °C for **TPB(2-TPTZ)**.

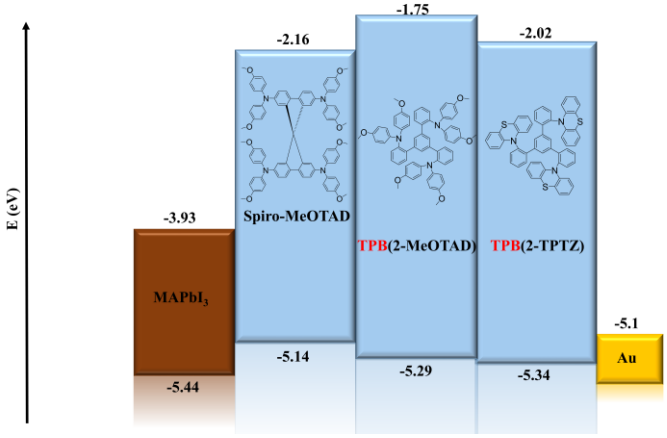

Fig. 4 Energy level diagram and device architecture of perovskite solar cells.

XRD analysis

The Powder X-Ray Diffraction (PXRD) patterns of **TPB(2-MeOTAD)** and **TPB(2-TPTZ)** were measured (Fig. S8). The PXRD plot for **TPB(2-TPTZ)** contained more well-defined and intense peaks than **TPB(2-MeOTAD)**. This indicates that **TPB(2-TPTZ)** has more crystalline character. It is possible that greater crystallinity would lead to decrease the π-π stacking distance, leading to increased intermolecular orbital interactions as we previously showed for the related compound based on SFX core.[6] Moreover, this would improve the mobility of holes through the material as has been presented for other materials with planar substituents like tetra- carbazole and phenothiazine substituted SFX with mobility as high as 1.57×10^{-3} $cm^2V^{-1}S^{-1}$ hole mobility of 2.08×10^{-3} $cm^2V^{-1}S^{-1}$, respectively.[37,38]

Photovoltaic performance

In order to investigate the suitability of **TPB(2-MeOTAD)** and **TPB(2-TPTZ)** as HTMs in perovskite solar cells, devices with a geometry (Fig. 4) of ITO/ETM/$MAPbI_3$/HTM/Au were fabricated, in which the HTM is either of the new materials or **Spiro-**

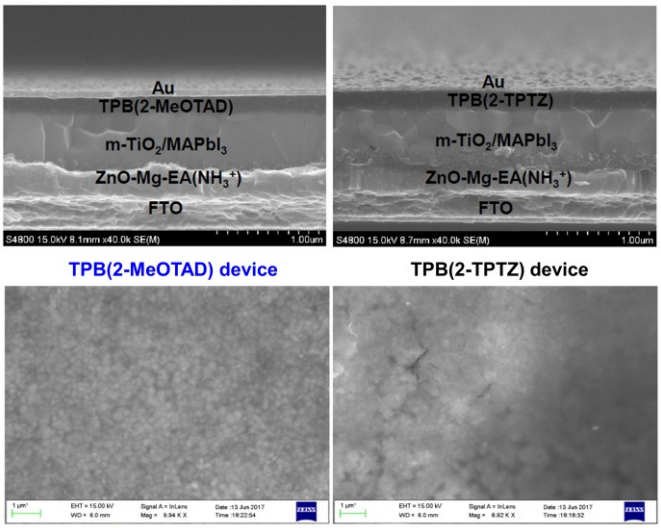

Fig. 5 Cross-sectional (top) and top-view (bottom) SEM images of PSCs with TPB-2-MeOTAD and TPB(2-TPTZ) as HTM.

OMeTAD as reference material. ZnO-Mg-EA(NH_3^+) layer acted as an effective ETM.[30] A detailed procedure is shown in the ESI.

Table 2. Device characteristics of the most efficient cells.

Name	J_{SC} /mA·cm^{-2}	V_{OC} /V	FF /%	η /%	R_S /Ω·cm^{-2}
TPB(2-MeOTAD)	19.32	0.97	64.54	12.14	9.10
TPB(2-TPTZ)	8.89	0.88	55.30	4.32	28.71

Better matched HOMO levels between the new materials and perovskite should facilitate efficient hole transfer and extraction with minimal energy loss. Additionally, the high LUMO energy level of **TPB(2-MePTAD)** (-1.75 eV) and **TPB(2-TPTZ)** (-2.02 eV) will effectively block electrons to prevent recombination at the anode. The cross-sectional view and top-view of the device is shown in Fig. 5; the thickness of photoactive layer is ≈700 nm and the HTL thickness is ≈200 nm. When the perovskite film is coated with our HTM materials uniform and smooth morphology is observed for TPB(2-MeOTAD), while for the cell with phenothiazine based material blurred and rough surface can be seen.

The current density-voltage (*J-V*) curves for the best devices based on the new HTMs were investigated under standard air mass (AM) 1.5 conditions and results are shown in Fig. S9. We have performed device optimization by testing different concentration of hole conductors being deposited. Solutions with 35 mg/ml concentration were found to lead to the best film quality according to SEM images and the highest efficiency in PSCs, for more information see ESI. The best-performing cell based on **TPB(2-MeOTAD)** exhibited efficiency of 12.14% while the cell based on **TPB(2-TPTZ)** 4.32% (see Table 2). Devices performance statistics of 18 individual cells at forward (FS) and reverse scan (RS) are shown in Fig. S11. The reference device based on **Spiro-MeOTAD** showed PCE of 18.04%, as shown in Fig. S13 (ESI). The hysteresis behaviour of the PSC devices with **TPB(2-MeOTAD)** and **TPB(2-TPTZ)** as HTMs are measured through forward and reverse scans. The corresponding incident photon-to-electron conversion efficiency (IPCE) spectra of TPB-based devices as well as the related integrated photocurrents of the champion solar cells is described in **Fig. S10**. The results show that the integrated photocurrents from the IPCE spectra match well with the measured J_{SC}. Stability studies showed that devices comprising TPB(2-TPTZ) as the HTM show greater stability over 300 hours retaining 85% initial efficiency (Fig. S15) under dark storage in a dry box, at 25 °C temperature and relative humidity of 30%. On the other hand, TPB(2-MeOTAD) and Spiro-MeOTAD based devices stability tests showed that 75% and 72% of initial efficiencies were retained, respectively. This indicates that faster degradation must be associated with higher hydrophilic dimethoxydiphenylamine substituent and stability superiority of more hydrophobic phenothiazine based HTM.

To further evaluate commercial viability of these newly developed hole conductors we have calculated cost-per-peak-Watt as a function of solar cell efficiency, according to the method reported by Osedach et al.[29] The curves presented in Fig. 6 clearly indicate that state-of-the-art HTM spiro-MeOTAD, even at very optimistic cost per gram of only 100$, will contribute more than 40% to the final module cost (assuming target module cost of 0.50 $ per Wp)[39] failing to fit the theme of inexpensive and scalable solar cell technology, even at efficiencies as high as 20%. On the other hand, due to the very low cost of TPB(2-TPTZ) implementation of this material in the solar cell delivers the lowest material cost per peak Watt contribution with prospects of further cost reduction to as low as 0.005 $/Wp if efficiency above 12% were achieved.

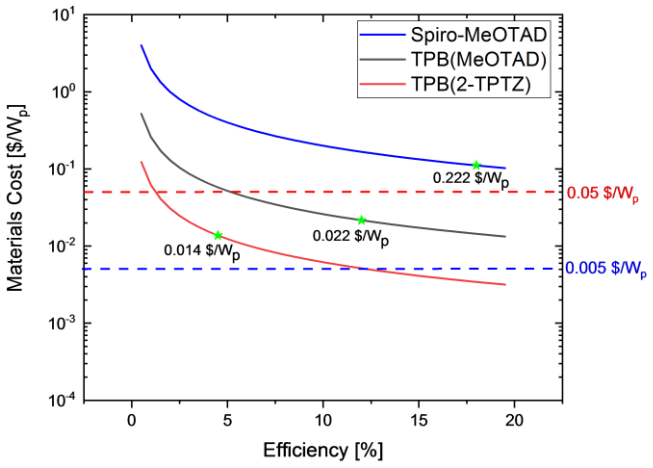

Fig. 6 Calculated material cost-per-peak-Watt ($ per Wp) as a function of solar cell efficiency. Star marks indicate device efficiencies delivered in this work.

Conclusions

These studies indicate that by using a triphenylbenzene core, the solubility of a HTM can be largely improved, relative to a spiro-carbon based material with the same substituents. Thus, more rigid and planar starting materials can be employed for HTM syntheses. In particular, we were able to use, for the first time, the phenothiazine unit to form a highly soluble hole transpor material. This demonstrates a route to employ a substituent with highly attractive properties including ultra-low cost, a desirable HOMO energy level and good rigidity for hole mobility and thermal stability.

These results underline the necessity of a broader look into designing materials as hole conductors for perovskite solar cells taking into account trade-offs between conversion efficiency, scalability and cost in order to deliver materials for large-scale production i.e. commercially viable. We therefore believe that our approach will be of broad interest as it is the first work to identify the use of phenothiazine to reduce the cost of functioning hole-transport materials in perovskite solar cells.

We acknowledge that further efficiency improvement is desirable, but believe that this initial report will be important in catalysing further work in this direction.

Conflicts of interest

There are no conflicts to declare.

Acknowledgements

M.R.M. and N.R. acknowledge European Union's Horizon 2020 Research and Innovation Programme H2020-MSCA-IF-2014-659237 for financial support.

Notes and references

1 W. S. Yang, B. W. Park, E. H. Jung, N. J. Jeon, Y. C. Kim, D. U. Lee, S. S. Shin, J. Seo, E. K. Kim, J. H. Noh and S. Il Seok, *Science (80-.).*, 2017, **356**, 1376–1379.

2 N.-G. Park, M. Grätzel, T. Miyasaka, K. Zhu and K. Emery, *Nat. Energy*, 2016, **1**, 16152.

3 Q. Han, Y.-T. Hsieh, L. Meng, J.-L. Wu, P. Sun, E.-P. Yao, S.-Y. Chang, S.-H. Bae, T. Kato, V. Bermudez and Y. Yang, *Science*, 2018, **361**, 904–908.

4 C. Kou, S. Feng, H. Li, W. Li, D. Li, Q. Meng and Z. Bo, *ACS Appl. Mater. Interfaces*, 2017, **9**, 43855–43860.

5 Z.-Z. Z. Sun, Y.-L. L. Xu, R. Zhu and H.-Y. Y. Liu, *Org. Electron. physics, Mater. Appl.*, 2018, **63**, 86–92.

6 M. Maciejczyk, A. Ivaturi and N. Robertson, *J. Mater. Chem. A*, 2016, **4**, 1–22.

7 J.-Y. Seo, H.-S. Kim, S. Akin, M. Stojanovic, E. Simon, M. Fleischer, A. Hagfeldt, S. M. Zakeeruddin and M. Grätzel, *Energy Environ. Sci.*, 2018.

8 M. A. Green, Y. Hishikawa, E. D. Dunlop, D. H. Levi, J. Hohl-Ebinger and A. W. Y. Ho-Baillie, *Prog. Photovoltaics Res. Appl.*, 2018, **26**, 3–12.

9 Y.-C. Chen, S.-K. Huang, S.-S. Li, Y.-Y. Tsai, C.-P. Chen, C.-W. Chen and Y. J. Chang, *ChemSusChem*, 2018, **11**, 3225–3233.

10 L. Wang, J. Zhang, P. Liu, B. Xu, B. Zhang, H. Chen, A. K. Inge, Y. Li, H. Wang, Y.-B. Cheng, L. Kloo and L. Sun, *Chem. Commun.*, 2018, **54**, 9571–9574.

11 Y. Li, K. R. Scheel, R. G. Clevenger, W. Shou, H. Pan, K. V. Kilway and Z. Peng, *Adv. Energy Mater.*, 2018, **8**, 1801248.

12 Š. Daškevičiū tė, N. Sakai, M. Franckevičius, M. Daškevičienė, A. Magomedov, V. Jankauskas, H. J. Snaith and V. Getautis, *Adv. Sci.*, 2018, **5**, 1700811.

13 A. Magomedov, S. Paek, P. Gratia, E. Kasparavicius, M. Daskeviciene, E. Kamarauskas, A. Gruodis, V. Jankauskas, K. Kantminiene, K. T. Cho, K. Rakstys, T. Malinauskas, V. Getautis and M. K. Nazeeruddin, *Adv. Funct. Mater.*, 2018, **28**, 1704351.

14 H. D. Pham, T. T. Do, J. Kim, C. Charbonneau, S. Manzhos, K. Feron, W. C. Tsoi, J. R. Durrant, S. M. Jain and P. Sonar, *Adv. Energy Mater.*, 2018, **8**, 1703007.

15 D. Li, J.-Y. Shao, Y. Li, Y. Li, L.-Y. Deng, Y.-W. Zhong and Q. Meng, *Chem. Commun.*, 2018, **54**, 1651–1654.

16 F. Zhang, S. Wang, H. Zhu, X. Liu, H. Liu, X. Li, Y. Xiao, S. M. Zakeeruddin and M. Grätzel, *ACS Energy Lett.*, 2018, **3**, 1145–1152.

17 X. Sun, Q. Xue, Z. Zhu, Q. Xiao, K. Jiang, H.-L. Yip, H. Yan and Z. Li, *Chem. Sci.*, 2018, **9**, 2698–2704.

18 N. J. Jeon, H. Na, E. H. Jung, T.-Y. Yang, Y. G. Lee, G. Kim, H.-W. Shin, S. Il Seok, J. Lee and J. Seo, *Nat. Energy*, 2018, **3**, 682–689.

19 L.-H. H. Xie, F. Liu, C. Tang, X.-Y. Y. Hou, Y.-R. R. Hua, Q.-L. L. Fan and W. Huang, *Org. Lett.*, 2006, **8**, 2787–90.

20 B. Xu, D. Bi, Y. Hua, P. Liu, M. Cheng, M. Grätzel, L. Kloo, A. Hagfeldt and L. Sun, *Energy Environ. Sci.*, 2016, **9**, 873–877.

21 K. Liu, Y. Yao, J. Wang, L. Zhu, M. Sun, B. Ren, L. Xie, Y. Luo, Q. Meng and X. Zhan, *Mater. Chem. Front.*, 2017, **1**, 100–110.

22 J. Qu, X. Jiang, Z. Yu, J. Lai, Y. Zhao, M. Hu, X. Yang and L. Sun, *Sci. China Chem.*, 2018, **61**, 172–179.

23 K. Pydzińska, P. Florczak, G. Nowaczyk and M. Ziółek, *Synth. Met.*, 2017, **232**, 181–187.

24 Z. Z. Sun, Y. L. Xu, R. Zhu and H. Y. Liu, *Org. Electron. physics, Mater. Appl.*, 2018, **63**, 86–92.

25 V. A. Chiykowski, Y. Cao, H. Tan, D. P. Tabor, E. H. Sargent, A. Aspuru-Guzik and C. P. Berlinguette, *Angew. Chemie - Int. Ed.*, 2018, **57**, 15529–15533.

26 H. Chen, W. Fu, C. Huang, Z. Zhang, S. Li, F. Ding, M. Shi, C.-Z. Li, A. K.-Y. Jen and H. Chen, *Adv. Energy Mater.*, 2017, **7**, 1700012.

27 K. Rakstys, S. Paek, G. Grancini, P. Gao, V. Jankauskas, A. M. Asiri and M. K. Nazeeruddin, *ChemSusChem*, 2017, **10**, 3825–3832.

28 K. Rakstys, S. Paek, M. Sohail, P. Gao, K. T. Cho, P. Gratia, Y. Lee, K. H. Dahmen and M. K. Nazeeruddin, *J. Mater. Chem. A*, 2016, **4**, 18259–18264.

29 T. P. Osedach, T. L. Andrew and V. Bulović, *Energy Environ. Sci.*, 2013, **6**, 711.

30 J. Cao, B. Wu, R. Chen, Y. Wu, Y. Hui, B. W. Mao and N. Zheng, *Adv. Mater.*, 2018, **30**, 1705596.

31 D. Trawny, M. Quennet, N. Rades, D. Lentz, B. Paulus and H.-U. Reissig, *European J. Org. Chem.*, 2015, **2015**, 4667–4674.

32 M. L. Petrus, M. T. Sirtl, A. C. Closs, T. Bein and P. Docampo, *Mol. Syst. Des. Eng.*, 2018, **3**, 734–740.

33 M. L. Petrus, T. Bein, T. J. Dingemans and P. Docampo, *J. Mater. Chem. A*, 2015, **3**, 12159–12162.

34 X. Liang, C. Wang, M. Wu, Y. Wu, F. Zhang, Z. Han, X. Lu, K. Guo and Y.-M. Zhao, *Tetrahedron*, 2017, **73**, 7115–7121.

35 S. S. Reddy, K. Gunasekar, J. H. Heo, S. H. Im, C. S. Kim, D. H. Kim, J. H. Moon, J. Y. Lee, M. Song and S. H. Jin, *Adv. Mater.*, 2016, **28**, 686–693.

36 C. M. Cardona, W. Li, A. E. Kaifer, D. Stockdale and G. C. Bazan, *Adv. Mater.*, 2011, **23**, 2367–71.

37 X. Liang, K. Wang, R. Zhang, K. Li, X. Lu, K. Guo, H. Wang, Y. Miao, H. Xu and Z. Wang, *Dye. Pigment.*, 2017, **139**, 764–771.

38 X. Liang, C. Wang, M. Wu, Y. Wu, F. Zhang, Z. Han, X. Lu, K.

Guo and Y. M. Zhao, *Tetrahedron*, 2017, **73**, 7115–7121.

39 D. ARPA-E (Washington), *$1/W Photovoltaic Systems White Paper to Explore a Grand Challenge from Solar*, 2010.